Cement and Concrete Research 41 (2011) 20–29

Contents lists available at ScienceDirect

Cement and Concrete Research

journal homepage: http://ees.elsevier.com/CEMCON/default.asp

Critical aspects of nano-indentation technique in application to hardened cement paste

D. Davydov *, M. Jirásek, L. Kopecký

Czech Technical University in Prague, Faculty of Civil Engineering, Department of Mechanics, Thákurova 7, Praha 6, 166 29, Czech Republic

ARTICLE INFO

Article history:
Received 22 December 2009
Accepted 2 September 2010

Keywords:
Calcium-silicate-hydrate (C–S–H) (B)
Elastic moduli (C)
Micromechanics (C)
Mechanical properties (C)
Statistical nanoindentation (B)

ABSTRACT

Several open questions related to the experimental protocol and processing of data acquired by the nano-indentation (NI) technique are investigated. The volume fractions of mechanically different phases obtained from statistical NI (SNI) analysis are shown to be different from those obtained by back-scattered electron (BSE) image analysis and X-ray diffraction (XRD) method on the same paste. Judging from transmission electron microscope (TEM) images, the representative volume element of low-density calcium-silicate hydrates (C–S–H) can be considered to be around 500 nm, whereas for high-density C–S–H it is about 100 nm. This raises the question how the appropriate penetration depth for NI experiments should be selected. Changing the maximum load from 1 mN to 5 mN, the effect of penetration depth on the experimental results is studied. As an alternative to the SNI method, a "manual" indentation method is proposed, which combines information from BSE and atomic-force microscopy (AFM), coupled to the NI machine. The AFM allows to precisely indent a high-density C–S–H rim around unhydrated clinkers in cement paste. Yet the results from that technique still show a big scatter.

1. Introduction

Nanoindentation (NI) is a widely used technique for measuring properties of materials at the micron and submicron levels. It consists in establishing contact between a substrate (sample) and an indenter with known properties and geometry. The force acting on the indenter is applied as the control variable and the corresponding penetration depth is recorded. Commonly, a trapezoidal loading program with loading, holding and unloading periods is used (Fig. 1b).

Elastic properties of the substrate can be evaluated from the unloading part of the load–penetration curve (Fig. 1a) by the standard Oliver–Pharr procedure [1] which determines the so-called indentation modulus(or reduced modulus) $M = E/(1-\nu^2)$, related to Young's modulus E and Poisson's ratio ν of the substrate, provided that the indentor is much stiffer than the substrate.

Another parameter commonly calculated from the indentation data is the hardness

$$H = \frac{P_{max}}{A_c} \tag{1}$$

where P_{max} is the maximum force and A_c is the contact area.

Although the described procedure is based on the assumption of material homogeneity, it has been applied to heterogeneous materials as well, using the so-called "grid" indentation method [2], also called the statistical nano-indentation method (SNI). The idea is to make a sufficiently large number of "random" indents (usually arranged in a regular grid) covering a certain representative area of the sample and then process the results statistically.

A more rigorous approach would be to select the indentation points such that they correspond to a certain phase. This will be called the "manual" indentation technique, because the exact position of the indentation points is to be set manually by the operator, and not automatically by the machine. The manual indentation technique will be applied here to the calcium-silicate-hydrate gel (C–S–H), and the results will be compared to the statistically processed results of the grid indentation method.

C–S–H, the main phase in the hardened cement paste, is a porous medium [2–5]. When applying the NI technique, it is important to choose the indentation depths correctly, so that the result is representative of the porous material behavior. If the indents are too small, the response is affected by surface roughness and is not representative of the particular phase. If the indents are too big, the results are affected by heterogeneities such as big capillary pores, unhydrated clinkers or other hydration products, and for very large indents actually yields the average properties of cement paste. The size of a representative volume element (RVE) of C–S–H can be estimated from transmission electron microscope (TEM) images (Fig. 2). The characteristic size of high-density C–S–H (C–S–H_{HD}) building blocks (globules) varies between 3–6 nm, while the diameter of low-density C–S–H (C–S–H_{LD}) fibers reaches 100 nm (Fig. 2c)! Moreover, the C–S–H_{LD} exhibits high porosity on the sub-micron

* Corresponding author.
E-mail address: denis.davydov@fsv.cvut.cz (D. Davydov).

0008-8846/$ – see front matter © 2010 Elsevier Ltd. All rights reserved.
doi:10.1016/j.cemconres.2010.09.001

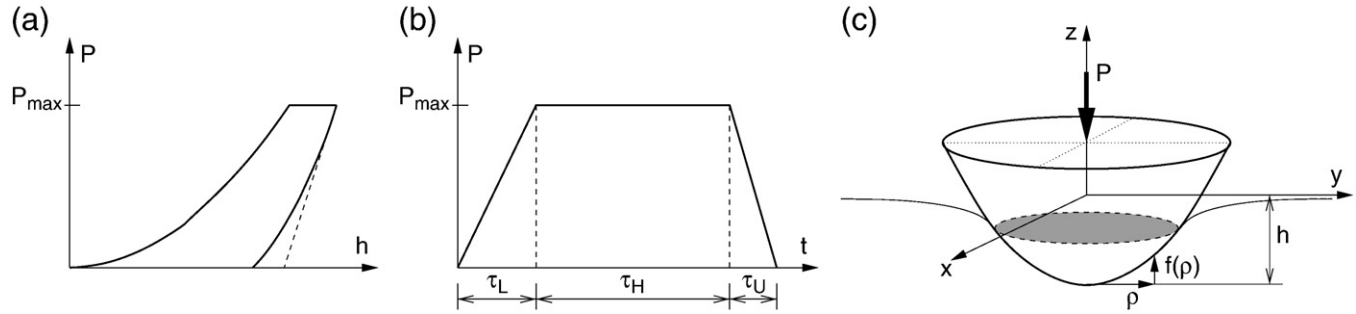

Fig. 1. a) Schematic illustration of the load–penetration curve; b) trapezoidal loading program used in a NI experiment; c) indentation of a substrate by a rigid axisymmetric indenter.

level. Therefore, indents in the range of 100–200 nm are deep enough to capture the mechanical behavior of C–S–H_{HD} phase only, whereas C–S–H_{LD} requires much deeper indents (probably around 500 nm). Indentation depths ranging between 100 and 200 nm are usually considered to be representative of both phases [2,3,5–11]. One of the aims of the current study is to investigate the size effect in NI.

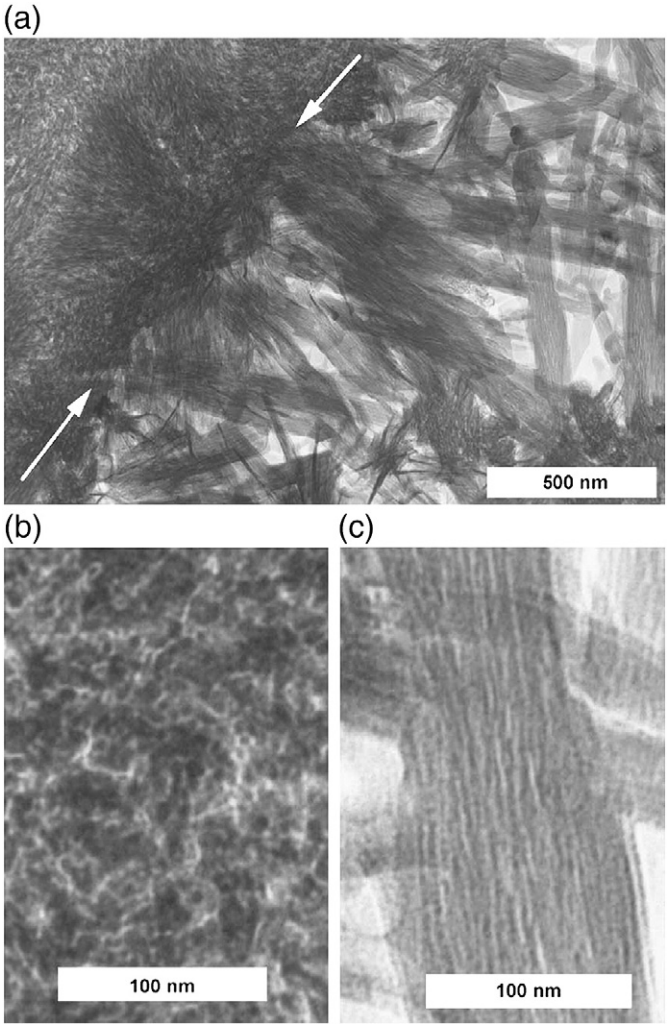

Fig. 2. (a) A transmission electron microscope (TEM) micrograph showing outer C–S–H and inner C–S–H present in a hardened C_3S paste with $w/c = 0.4$ hydrated at 20 °C for 8 years. White arrows indicate the boundary between inner C–S–H and outer C–S–H; the inner C–S–H is in the upper left part of the micrograph. (b) An enlargement of a region of inner C–S–H. (c) An enlargement of a fibril of outer C–S–H (reprinted with permission from [12]).

During the SNI analysis, the obtained results are described by a combination of Gaussian distributions with weight factors that are usually considered to be equal to the volume fractions of mechanically different phases. These results can be compared with volume fractions obtained by back-scattered electron (BSE) image analysis and X-ray diffraction (XRD). To the best of the authors' knowledge, such a comparison has never been done for cement paste.

In this paper, the following aspects are covered:

1. The effect of the penetration depth on NI results (i.e., the issue of RVE size for C–S–H phase).
2. The comparison of the well established statistical (grid) indentation technique with the proposed "manual" approach, which allows to access the real properties of a single phase with the minimum possible bias due to the heterogeneous nature of the sample.
3. The comparison of volume fractions obtained from SNI method to BSE and XRD. Given a reliable volume fraction, the estimate of C–S–H elastic properties is studied using the self-consistent (SC) homogenization scheme and the results from deep ($\approx$3 μm) indents.

2. Materials and preparation

For the present study, two types of cement were used, both mixed at water-cement ratio $w/c = 0.4$:

1. AALBORG white cement (C_3S 67.3, C_2S 23.3, C_4AF 0.4, C_3A 3.6, C 0.6, gypsum, hemihydrate, anhydrite 4.3, Fe_2O_3 0.3, Na_2O equivalent 0.19).
2. Pure alite cement.

The cumulative particle size distribution (PSD) for white cement is presented in Fig. 3.

All samples were cured for 1 day in room conditions, then demolded and stored in saturated conditions. Before NI, a small,

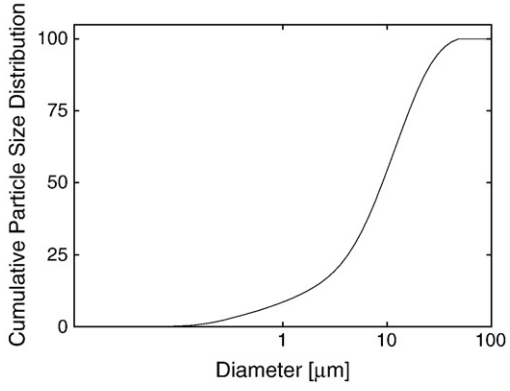

Fig. 3. Cumulative particle size distribution for Aalborg white cement.

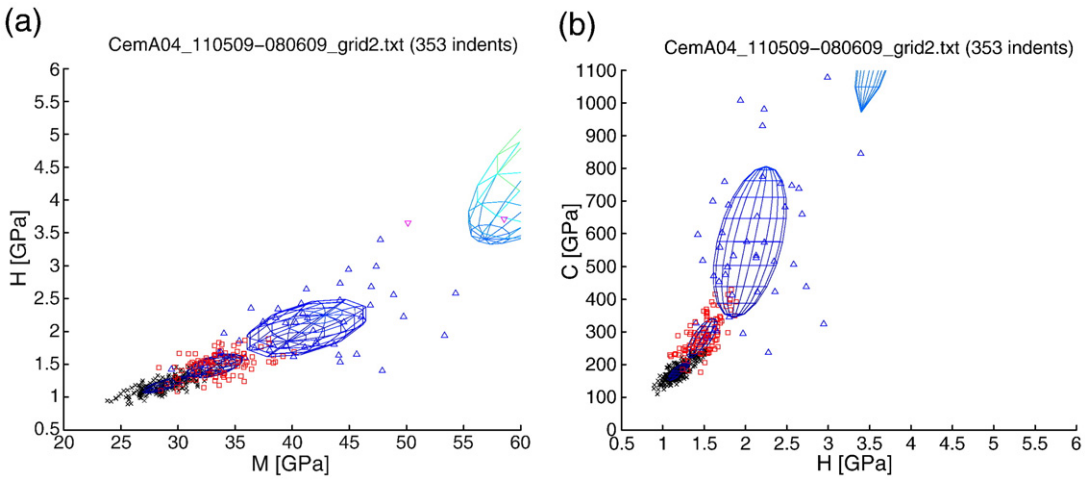

Fig. 4. Example of Gaussian mixture deconvolution of NI data with clustering: a) plane of parameters M and H, b) plane of parameters H and C.

coin-size sample was cut using a diamond saw. After that it was left for about 1 h in room conditions and then manually polished using Struers silicon-carbide papers of 100, 2000 and 4000 finenesses. Before indentation, the sample was cleaned for 2 min in ultrasonic bath. The resulting root-mean-square roughness, measured by Hysitron Nanoindenter on the 60 μm area with 1 Hz scanning rate after average plane subtraction, was 30–40 nm for all samples, which is sufficient for 150 nm and deeper indentation [10].

A Berkovich tip was used in all NI experiments reported here. The tip area function was calibrated on a silica sample using the standard procedure [13]. Four grids, each with 10×10 indents (400 indents in total) with 30 μm step, were used for each study. The indentation of each grid took about 8 h. After the processing of each grid, the Hysitron Nanoindenter was recalibrated by "air indents" [13] and the samples were repolished in order to decrease the effect of carbonation.

Four loading programs, which all had the same loading/unloading rate and dwelling period but differed by the maximum load, were applied:

1. 1-30-1/1: 1 second of loading up to 1 mN, 30 s of holding constant force, 1 s of unloading;
2. 2-30-2/2: 2 s of loading up to 2 mN, 30 s of holding constant force, 2 s of unloading;
3. 4-30-4/4: 4 s of loading up to 4 mN, 30 s of holding constant force, 4 s of unloading;
4. 5-30-5/5: 5 s of loading up to 5 mN, 30 s of holding constant force, 5 s of unloading.

3. Methods

According to the conventional Oliver–Pharr procedure [1], the indentation modulus $M = E/(1-\nu^2)$ and the hardness $H = P_{max}/A_c$ can be evaluated from the NI curve. Following Vandamme [2], an additional parameter

$$C = \frac{P_{max}}{2a_u x_1} \tag{2}$$

which characterizes long-term creep, was calculated from the data recorded during the holding period. In Eq. (2), a_u is the radius of contact before unloading and x_1 is a parameter obtained by fitting the evolution of penetration depth during the holding period by the function $h(t_L+t)-h(t_L) = x_1 ln(x_2 t+1)+x_3 t+x_4$. In [2], the purpose of parameter x_3 was to capture the thermal drift of the CSM nanoindenter used in that study. The present results have been obtained on the Hysitron machine, which measures the thermal drift before each NI and subtracts its influence from the measured results. Therefore, x_3 can be set to zero.

In total, three parameters (M, H and C) are evaluated from one indent. A statistically representative set of indents can be analyzed

Table 1
Results of SNI analysis of 20×20 indents at 20 μm spacing under 2–30–2/2 mN loading performed on white cement at age 28 days. μ_i, S_i and f are mean values, covariance matrices and weights (volume fractions) for each phase in the M–H–C space.

	Grid 1				Grid 2			
	M [GPa]	H [GPa]	C [GPa]	f [−]	M [GPa]	H [GPa]	C [GPa]	f [−]
μ_1	30.10	1.25	186.44	0.55	28.88	1.19	180.81	0.53
	5.09	0.27	60.88		4.69	0.24	51.13	
S_1	0.27	0.02	3.87		0.24	0.02	3.29	
	60.88	3.87	1083.36		51.13	3.29	871.66	
μ_2	36.23	1.55	304.15	0.30	33.23	1.48	281.49	0.31
	21.49	0.77	226.10		6.28	0.26	84.29	
S_2	0.77	0.05	12.26		0.26	0.04	8.19	
	226.10	12.26	5100.02		84.29	8.19	3688.56	
μ_3	40.87	2.10	567.49	0.10	41.26	2.05	575.32	0.13
	67.42	3.13	1614.42		29.64	1.22	382.66	
S_3	3.13	0.26	62.19		1.22	0.20	45.59	
	1614.42	62.19	49628.80		382.66	45.59	53459.88	
μ_4	62.45	4.68	2483.15	0.05	65.88	4.94	2571.19	0.04
	272.45	24.56	30997.38		112.08	13.27	14277.85	
S_4	24.56	2.70	3483.29		13.27	2.61	2458.64	
	30997.38	3483.29	5133517.05		14277.85	2458.64	2551367.28	

Table 2
Results of SNI analysis (Table 1) in terms of coefficients of variation ((4), diagonal terms) and Pearson's correlation coefficients ((5), off-diagonal terms).

	Grid 1			Grid 2		
	M [%]	*H* [%]	*C* [%]	*M* [%]	*H* [%]	*C* [%]
1	7	84	82	7	81	80
	84	11	83	81	11	81
	82	83	18	80	81	16
2	13	74	68	8	56	55
	74	15	76	56	13	72
	68	76	23	55	72	22
3	20	75	88	13	50	30
	75	24	55	50	22	44
	88	55	39	30	44	40
4	26	91	83	16	78	84
	91	35	94	78	33	95
	83	94	91	84	95	62

assuming that the distribution of each parameter is a combination of several Gaussian distributions, each corresponding to a different phase. The probability density function of these three parameters collected in a column matrix $x=(M,H,C)^T$ is thus written as

$$f(x)=\sum_{k=1}^{P}\frac{f_k}{\sqrt{det(2\pi\mathbf{S}_k)}}exp\left(-\frac{1}{2}(\mathbf{x}-\boldsymbol{\mu}_k)\cdot\mathbf{S}_k^{-1}\cdot(\mathbf{x}-\boldsymbol{\mu}_k)\right) \quad (3)$$

where P is the number of phases, f_k is the volume fraction of phase k, $\boldsymbol{\mu}_k$ are the mean values of the parameters in phase k, and $\mathbf{S}_k$ is the 3×3 covariance matrix, which was previously considered as diagonal [2]. Inspired by the idea privately communicated by F.-J. Ulm [14], we deal with a general non-diagonal matrix, which means that the variables M, H and C are not considered as statistically independent. This is more realistic, since some correlation among the mechanical properties can certainly be expected.

The Expectation Maximization (EM) algorithm was used to obtain the maximum likelihood estimates of the parameters in a Gaussian mixture model using Matlab. The number of phases (i.e., of Gaussian distributions combined in the mixture) was set to $P=4$ and kept constant during all estimates for the ease of comparison. The first two phases (with the lowest mean values of indentation modulus and hardness) are assumed to be low- and high-density C–S–H. The third phase corresponds to portlandite (calcium hydroxide, CH), and the fourth phase does not seem to have a direct physical meaning, as will be explained later. After estimation of the parameters, clustering can be performed, and each indent is attributed to one of the phases. An example of Gaussian mixture deconvolution in 3D in presented in Fig. 4. The ellipsoids (projected as ellipses) are multidimensional analogues of confidence intervals. The fact that the ellipses in the H–M plane are elongated and their major axes are inclined indicates that there is a strong correlation between these parameters, i.e., hardness and indentation modulus.

Table 3
Volume fraction of phases determined by SNI, BSE and XRD on white cement at age 28 days.

Vol.%	Porosity	C–S–H	CH	Clinker
SNI Grid 1	n.a.	85	10	n.a.
SNI Grid 2	n.a.	84	13	n.a.
BSE	4	66	18	10
XRD	n.a.	53	21	15

4. Results and discussion

4.1. Repeatability of SNI and packing-density fit

Before starting the analysis of experimental results, the repeatability of the considered experimental procedure and evaluation technique needs to be checked. For this purpose, 400 indents in a 20×20 grid with 20 μm spacing were performed twice on the same white cement sample at age 28 days under loading program 2-30-2/2. The results are presented in Table 1. The resulting differences between the mean values of parameters obtained from the two grids are below 10%.

More insight into the statistical properties of the results is provided by characteristics such as the coefficients of variation and Pearson's correlation coefficients. The coefficient of variation of parameter i ($i=1,2,3$ corresponds respectively to parameters M, H and C) for phase k is defined as

$$\mathrm{CoV}_{k,i}=\frac{\sqrt{S_{k,ii}}}{\mu_{k,i}}\times100\% \quad (4)$$

and is a normalized measure of scatter of that parameter.

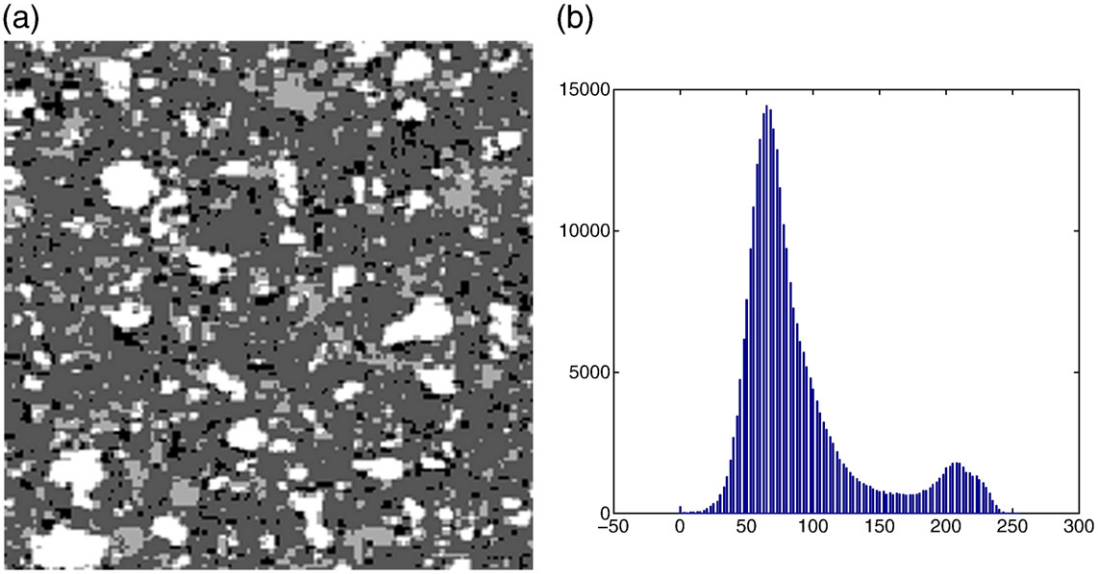

Fig. 5. BSE image analysis: a) 200×200 μm^2 (144×144 px) crop of the 1250×850 μm^2 image; b) image histogram.

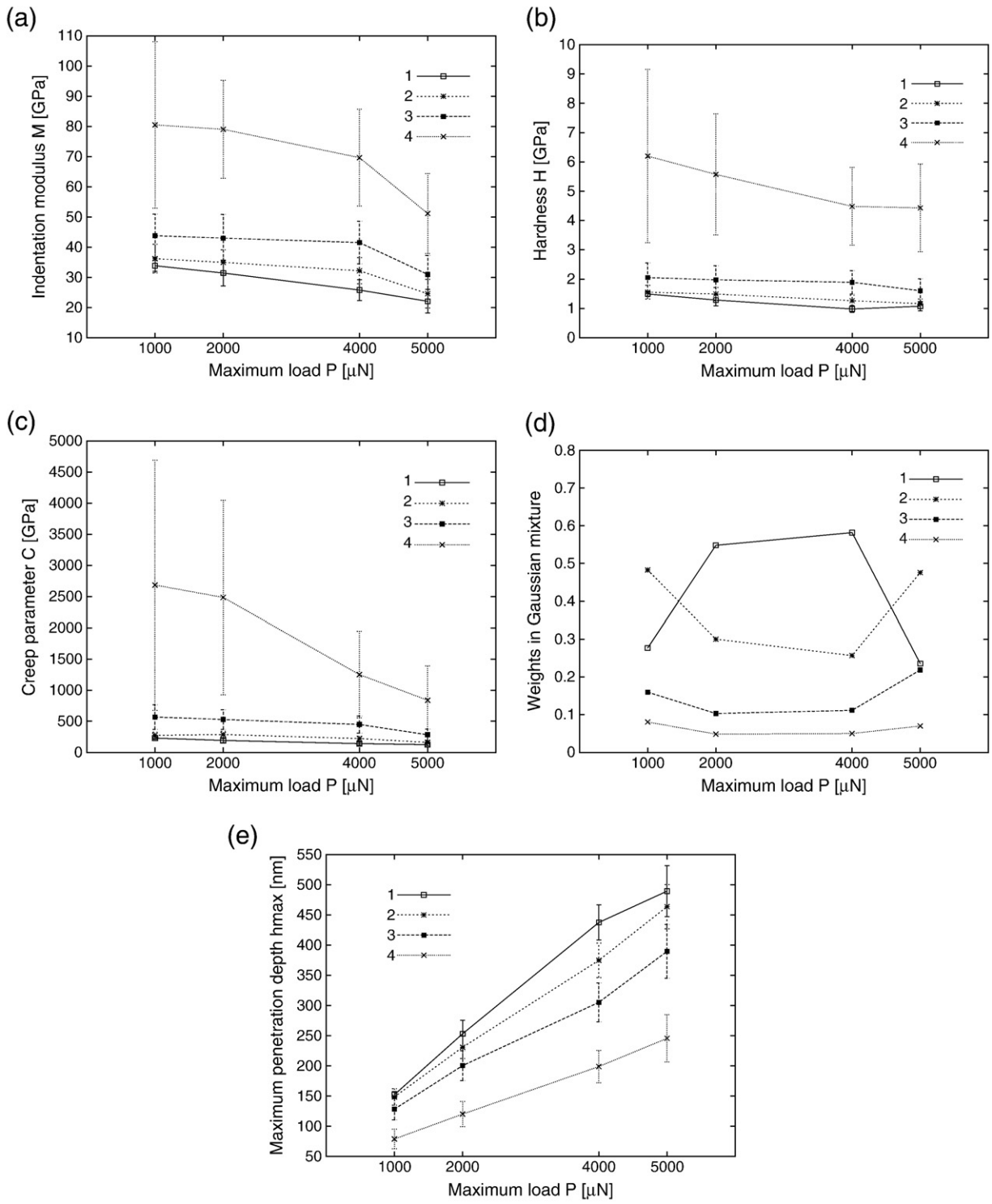

Fig. 6. Results of SNI with four phases depending on maximum load: a) Indentation modulus, b) hardness, c) creep parameter, d) weights in Gaussian mixture model, e) maximum penetration depth. Error bars represent standard deviation.

Table 4
Self-consistent homogenization of cement paste elastic properties based on XRD volume fractions compared with results from NI at the level of cement paste.

	M	E	ν
SC: 20 GPa	22.37	23.75	0.24
SC: 25 GPa	25.84	27.46	0.24
SC: 30 GPa	29.04	30.88	0.24
NI: $P=90$ mN, $h\approx 3$ μm	25 ± 5	n.a.	n.a.

Pearson's correlation coefficient is calculated for each pair of parameters ($i\neq j$) for phase k as

$$PCC_{k,ij} = \frac{S_{k,ij}}{\sqrt{S_{k,ii}S_{k,jj}}} \times 100\% \quad (5)$$

The Pearson coefficient would be 100% if the two parameters were directly linked by a linear increasing function. Table 2 presents

these coefficients calculated for each phase from Table 1. The CoV's of indentation modulus M and hardness H are found to be relatively low, while the CoV of creep parameter C is higher, especially for phase 4. All the PCC's are positive and quite high, which indicates a strong positive correlation between each two properties. This means that if the material near a certain indent is stiffer, it is in general also harder and exhibits less creep. The assumption of statistical independence between the properties would not be realistic.

4.2. Comparison of SNI volume fractions with data from BSE and XRD

From the results in Table 1 it is clear that SNI does not capture the properties of unhydrated clinkers, which are known to have elastic

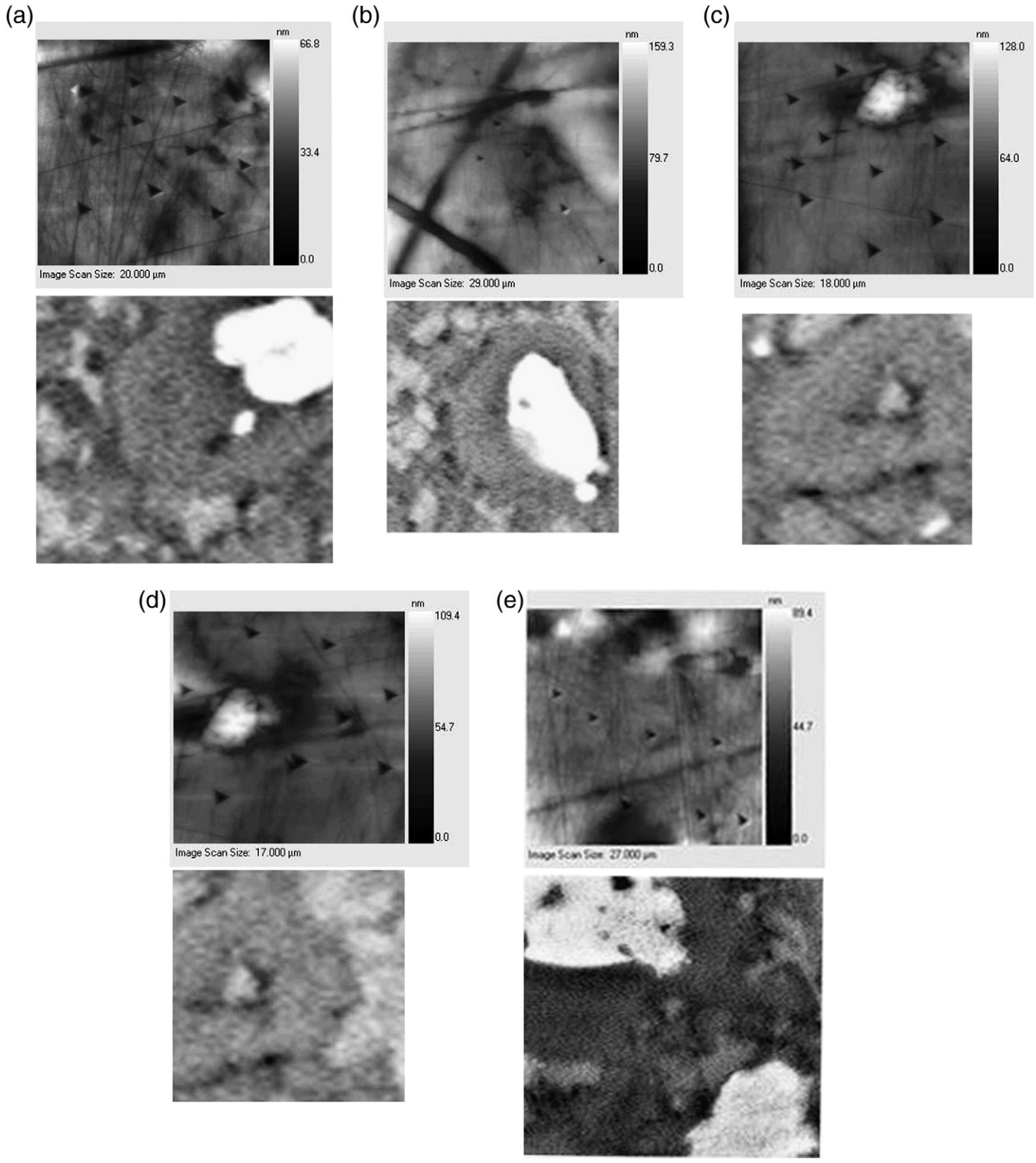

Fig. 7. BSE (bottom) and AFM (top; after indentation; average plane is subtracted) images illustrating the proposed manual indentation technique and the choice of NI points for white Aalborg cement paste with $w/c = 0.4$.

moduli around 130 GPa. The fourth phase in our analysis (with mean value of indentation modulus near 64 GPa) corresponds to artifacts of the method. The reason is that clinkers are embedded in porous matrix and therefore this heterogeneity, as it has been studied in [15], leads to bias in determination of elastic moduli. Porosity, in the authors' opinion, can be captured by SNI as a single phase only if present in high volume fractions, which leads to a considerable shift of the obtained elastic properties towards lower values. Otherwise, it becomes impossible to distinguish by SNI between sound hydration products and their mixture with porosity, which is the case here.

In order to extend this investigation, further comparison can be done with the analysis of Back-Scattered Electron (BSE) images and results of X-Ray diffraction (XRD). XRD results were provided by Vanessa Kocaba (EPFL, Switzerland) in terms of mass fractions. They were recalculated into volume fractions based on known densities of individual phases. Since pores cannot be detected by this technique, the volume fractions are considered as the volume of each phase divided by the total volume of the solid material (excluding pores). A BSE image of white cement of size 1250×850 μm with resolution 0.57 pix/μm was used. The image was segmented into 4 regions according to the gray level: 0–45, 46–95, 96–170 and 170–255, where 0 means black and 255 means white. These regions respectively correspond to porosity, C–S–H, portlandite and unhydrated clinker. The threshold 170 of the last region (clinker) was chosen according to the local minimum in the histogram (similar to [16]), whereas the first two were estimated by visual inspection of the image. The results of segmentation and the image histogram are presented in Fig. 5.

It is clearly seen that the volume fractions obtained by SNI do not agree with those obtained by XRD and BSE (Table 3). We consider XRD results to be the closest to reality. The difference in volume fractions of C–S–H determined by XRD and BSE is most likely due to the low resolution of the BSE image used. By covering the same area with several pictures, more porosity could be distinguished and therefore less area would be attributed to C–S–H.

Based on this comparison we can conclude that the volume fractions obtained by SNI are not representative of separate phases in cement paste, even though they are repeatable. What is mechanically tested by indentation is most probably a mixture of hydration product phases, which leads to mechanically different media. Since the modulus of CH is known to be around 40 GPa [17], we can conclude that the third peak indeed represents CH but only partly. The rest is mixed with C–S–H. This hypothesis is also confirmed by a recent XRD study of nanoindentation points [18].

4.3. Choice of penetration depth

The mechanical properties obtained from NI experiments might be affected by the penetration depth reached in the tests. For crystalline materials such as metals, it is well known that the hardness determined by NI exhibits a strong dependence on the indentation depth, as observed for a flat punch already by Ashby [19]. This phenomenon can be attributed to the development of geometrically necessary dislocations beneath the indenter. For a conical indenter, the size effect on hardness was studied by Nix and Gao [20] and Huang et al. [21]. Swadener et al. [22] extended this work to indenters of different sizes and shapes. A general shape/size effect law for hardness was proposed by Pugno [23].

For cement paste, Němeček [24] reported a strong size effect on elastic properties measured by NI and evaluated by the standard Oliver–Pharr [1] procedure from loading–unloading tests with no dwell period at the peak load.

Usually, the maximum force is prescribed as a control variable, and the depth depends on the selected load level. Several loading programs with maximum force ranging from 1 to 5 mN were used to study this effect. The resulting penetration depths range from 150 nm to 600 nm.

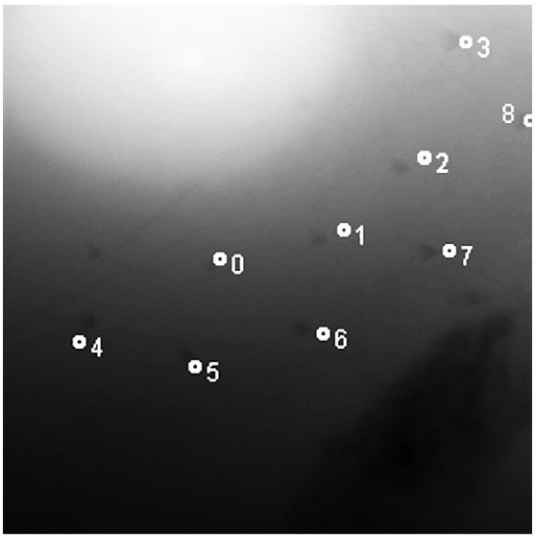

Fig. 8. AFM image with prescribed points for NI in Hysitron software. The scan size is 34 μm.

From Fig. 6 we can see that different penetration depths lead to very different results. This cannot be explained by the surface roughness effect only, since the deviation from an ideal plane (in the root-mean-square sense) is 30 nm in all samples, i.e., small enough to provide unbiased results even at low load levels.

The discrepancies can probably be explained as follows: For deeper indents, the effect of nearby porosity is stronger, which leads to a shift of elastic modulus and hardness towards smaller values. The question is, how deep should one indent be, in order to obtain representative properties of C–S–H_{LD}. Loading up to 5 mN is definitely too high since it even shifts the third peak from 40 GPa to 30 GPa (compared to 4 mN loading) and the first two are too close (22 and 24 GPa) to have a distinct physical meaning (Fig. 6).

Another possible explanation is the influence of damage. The deeper we indent, the more damage is induced, and therefore the decrease of elastic properties is more pronounced; see the results for 2 and 4 mN loading in Fig. 6.

In order to shed some light on this matter, we produced 100 indents into the same paste using the 60–30–60/90 mN loading program, which results in penetration depths about 3 μm and thus represents the homogenized properties of cement paste. We can take three volume fractions from XRD analysis (Table 3) and assume that the rest is

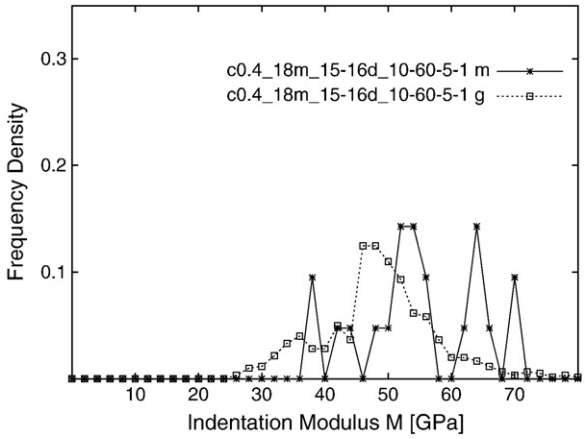

Fig. 9. Comparison of the "grid" (*g*, 600 random indents) and "manual" (*m*, 21 indents into C–S–H_{HD}) indentation techniques on a white cement paste sample $w/c=0.4$, hydrated for 18 months in saturated conditions; the time of exposure to room conditions is around 14 days.

attributed to porosity. Then, using typical elastic properties of CH ($E=38$ GPa and $\nu=0.305$), clinker ($E=130$ GPa, $\nu=0.3$) and porosity ($E=0$ GPa, $\nu=0$), we can check the effect of different elastic moduli of C–S–H (keeping its $\nu=0.24$) on the elastic properties of cement paste using the self-consistent homogenization scheme [25,26]. This can be compared to the indentation moduli extracted from deep indents (Table 4).

We can conclude that the mean properties of C–S–H (weighted average of C–S–H_{LD} and C–S–H_{HD}) should be around 25 GPa. This proves indirectly that the results obtained from the 4-30-4/4 mN loading are the most realistic ones for both C–S–H phases. Yet it has to be stressed that the volume fractions obtained from this loading are different from those obtained from XRD analysis.

4.4. "Manual" and "grid" indentation methods

In order to increase the accuracy of the "grid" indentation method, a new "manual" method is used. The main idea, already proposed in [27,28], is to choose the position of indentation points in advance such that NI would "hit" a particular phase and thus increase the accuracy of the obtained results. This approach will be illustrated on the C–S–H_{HD} phase.

Using BSE images, C–S–H_{HD} can be identified as a rim around the unhydrated clinker. Based on a BSE image, several preferred regions were chosen for NI (Fig. 7). Then these regions were detected in the optics of the Hysitron NI machine. A precise navigation and choice of NI points was done in an atomic force microscope (AFM), which is coupled with NI. Since the output from AFM is a height profile, it is impossible to distinguish between different phases. However, clinkers, which have a much higher elastic modulus, are represented by "elevations" in AFM, and also certain scratches could be identified. Comparing this information to the BSE image, 5–9 points for NI were reasonably prescribed on the area of about 20–30 μm^2 (Fig. 7). Unfortunately, the accuracy of the Hysitron Tribo Indenter on such areas is not sufficient to "hit" exactly the prescribed points (Fig. 8). Therefore, the area was scanned again after each series

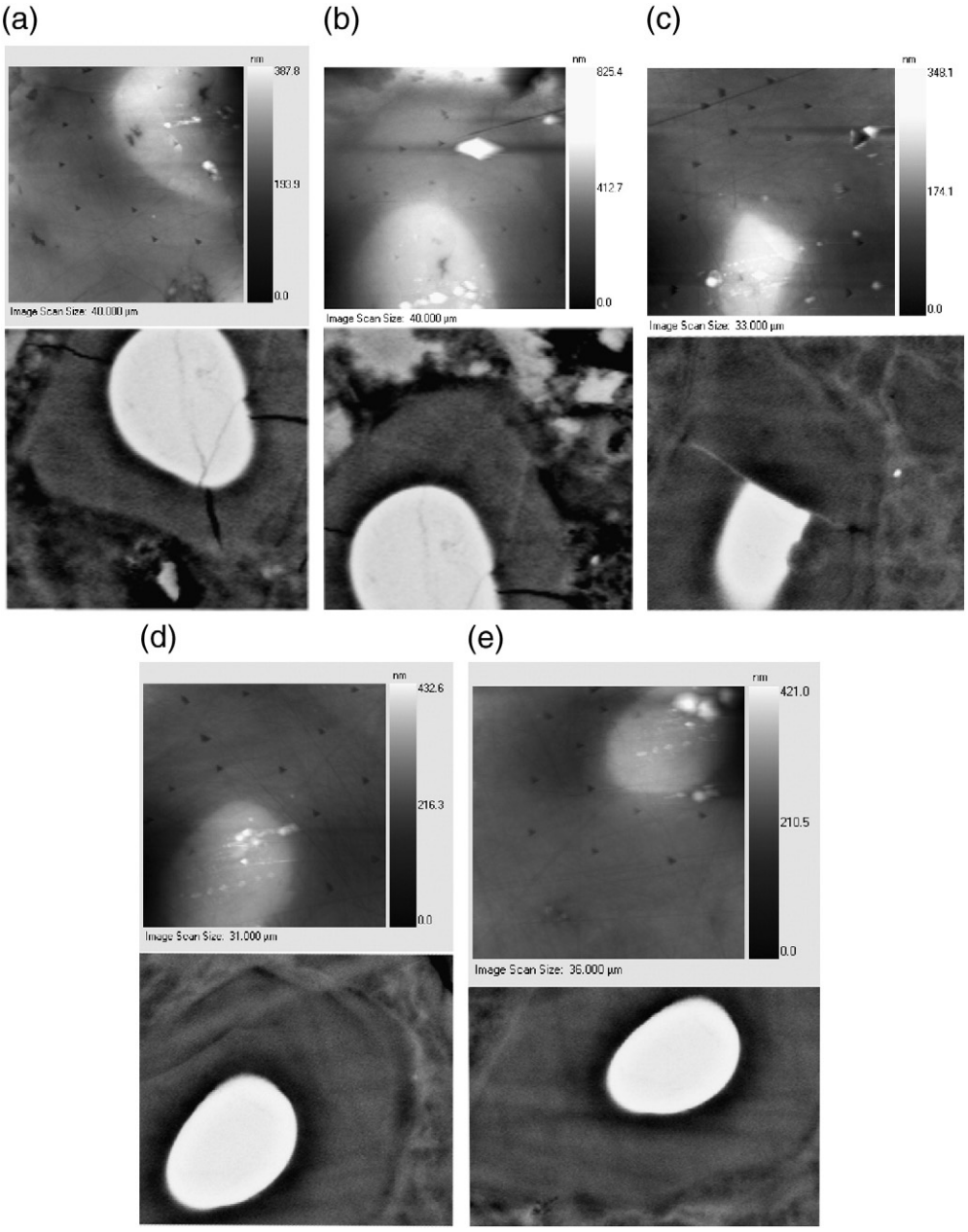

Fig. 10. BSE (bottom) and AFM (top; after indentation; average plane subtracted) images showing the regions selected for C–S–H_{HD} indentation of alite paste.

and only indents which really went into C–S–H_{HD} were used in the analysis.

The described method was applied to the white Aalborg cement paste mixed at $w/c = 0.4$. The total number of indents made by the "manual" method was 63. A filtering procedure reduced the total number of indents to 22. The loading program 10–60–5/1 mN was used, and the resulting penetration depths were 126 ± 16 nm. Histograms of the indentation modulus M obtained from the "grid" indentation technique and manual indentation technique performed on C–S–H_{HD} are compared in Fig. 9.

We can see that even when the indents are precisely pointed into the C–S–H_{HD} phase, the results show a big scatter. A part of the histogram with indentation moduli higher than 60 GPa could be explained by the proximity of the grain, which could happen to be under the indentation point in some cases. In order to account for those indents, it is proposed to apply a second loading cycle and compare the indentation moduli obtained from two unloading curves. The increase of M with the penetration depth can be considered as an indication of a clinker in the vicinity of the indentation point. A considerable decrease can be attributed to big capillary pores nearby.

Using the proposed approach, a sample of alite paste mixed at $w/c = 0.4$ was studied as well. The loading program was 10-100-5/1 mN, the resulting penetration depths were 230 ± 49 nm. After a filtering procedure, 72 indents into C–S–H_{HD} were used (Fig. 10). The obtained histogram of indentation modulus is presented in Fig. 11.

The indentation moduli obtained on alite paste are considerably different from the properties of C–S–H_{HD} obtained on white Aalborg cement paste with $w/c = 0.4$ (Fig. 9). An effect of mixture of CH and C–S–H manifests itself by a peak in the indentation moduli around 40 GPa (Fig. 11). That is obvious if we recall that the indentation was done only in what appears as C–S–H_{HD}, yet the obtained values of indentation moduli actually correspond to CH.

5. Conclusion

The following conclusions can be drawn:

1. The agreement between volume fractions obtained by SNI method, BSE image analysis and XRD is poor. Therefore, what is tested by SNI is not only pure phases (like CH with known elastic properties around 40 GPa), but their mixture, particularly C–S–H and CH. That is why the volume fraction of CH from SNI is less than that obtained from XRD and BSE.
2. The manual indentation method clearly shows the complexity of the properties of the C–S–H rim around an unhydrated grain, confirming again the hypothesis of mixture of C–S–H and CH. In the case of Alite paste, two distinct peaks in the histogram can be attributed to C–S–H_{HD} (around 30 GPa) and a mixture of C–S–H_{HD} and CH (around 40 GPa). Application to cement paste shows a much bigger scatter.
3. An increase of penetration depths leads to a general shift in NI results toward lower elastic moduli. Possible explanations are:
   - The surface roughness is too high for 1 mN indents.
   - There is an effect of damage (2 mN and 4 mN loading).
   - The change of effective media with the increase of indentation depth by increasing the effect of large capillary pores in the vicinity of the indentation point. 500 nm deep indents are shown to lead to a noticeable artificial decrease of the obtained elastic properties, thus the results obtained from such deep indents cannot be trusted.
   - The fact that the RVE size of C–S–H_{LD} is around 500 nm, based on a TEM image (Fig. 2), leads to the necessity of penetration depths bigger than usually used ($\approx$200 nm) in order to capture the representative properties of C–S–H_{LD}.
4. C–S–H properties obtained by the 4–30–4/4 mN loading are in the best agreement with the estimated mean elastic properties of the C–S–H phase. This estimate is based on the comparison of results from very deep (about 3 μm) indents and the results of SC homogenization of cement paste elastic properties based on XRD volume fractions.

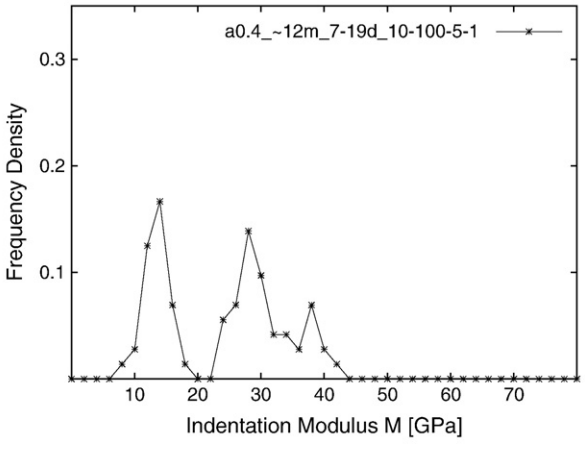

Fig. 11. Indentation moduli histogram for alite sample with $w/c = 0.4$, $h_{max} = 230 \pm 49$ nm (72 indents).

Acknowledgments

The authors are grateful to the European Community for the full support of Denis Davydov under the Marie Curie Research Training Network MRTN-CT-2005-019283 "Fundamental understanding of cementitious materials for improved chemical, physical and aesthetic performance" and to the Ministry of Education, Youth and Sports of the Czech Republic for the full support of Milan Jirásek under the Research Plan MSM6840770003 and full support of Lubomír Kopecký under the Research Plan MSM6046137302. We are also grateful to our colleagues at Vienna University of Technology, particularly to Christian Pichler, who performed comparative indentations on our sample in their laboratory.

References

[1] W. Oliver, G. Pharr, An improved technique for determining hardness and elastic modulus using load and displacement sensing indentation experiments, Materials Research 7 (1992) 1564–1582.
[2] G. Constantinides, F.-J. Ulm, The effect of two types of C–S–H on the elasticity of cement-based materials: Results from nanoindentation and micromechanical modeling, Cement and Concrete Research 34 (2004) 67–80.
[3] H. Jennings, J. Thomas, J. Gevrenov, G. Constantinides, F.-J. Ulm, A multi-technique investigation of the nanoporosity of cement paste, Cement and Concrete Research 37 (2007) 329–336.
[4] A. Allen, J. Thomas, H. Jennings, Composition and density of nanoscale calcium-silicate-hydrate in cement, Nature Materials 6 (2007) 311–316.
[5] G. Constantinides, F.-J. Ulm, The nanogranular nature of C–S–H, Journal of the Mechanics and Physics of Solids 55 (2007) 64–90.
[6] C. Pichler, R. Lackner, F.-J. Ulm, Identification of logarithmic-type creep of Calcium–Silicate–Hydrates (CSH) by means of nanoindentation, Strain 45 (1) (2008) 17–25.
[7] W. Zhu, J. Hughes, N. Bicanic, C. Pearce, Nanoindentation mapping of mechanical properties of cement paste and natural rocks, Materials Characterization 58 (2007) 1189–1198.
[8] L. Sorelli, G. Constantinides, F.-J. Ulm, F. Toutlemonde, The nano-mechanical signature of Ultra High Performance Concrete by statistical nanoindentation techniques, Cement and Concrete Research 38 (2008) 1447–1456.
[9] M. DeJong, F.-J. Ulm, The nanogranular behavior of C–S–H at elevated temperatures up to 700 °C, Cement and Concrete Research 37 (2007) 1–12.
[10] M. Miller, C. Bobko, M. Vandamme, F.-J. Ulm, Surface roughness criteria for cement paste nanoindentation, Cement and Concrete Research 38 (4) (2008) 467–476.
[11] A. Jager, R. Lackner, J. Eberhardsteiner, Identification of viscoelastic properties by means of nanoindentation taking the real tip geometry into account, Meccanica 42 (2007) 293–306.
[12] I. Richardson, Tobermorite/jennite- and tobermorite/calcium hydroxide-based models for the structure of C–S–H: applicability to hardened pastes of tricalcium silicate, β-dicalcium silicate, Portland cement, and blends of Portland cement with

blast-furnace slag, metakaolin, or silica fume, Cement and Concrete Research (34) (2004) 1733–1777.
[13] Hysitron Inc., User manual, NRL-M-100 v. 8.1.1, Minneapolis, USA, http://www.hysitron.com.
[14] F.-J. Ulm, Private communication at NICOM3 conference, Prague, June 2009.
[15] P. Kabele, D. Davydov, P. Jún, J. Němeček, M. Jirásek, Study of micromechanical behavior of cement paste by integration of experimental nanoindentation and numerical analysis, in: H.M.R. Tada-aki Tanabe, Kenji Sakata (Eds.), Creep, shrinkage and durability mechanics of concrete and concrete structures: Proceedings of the CONCREEP 8 conference, Ise-Shima, Japan, 2009, pp. 89–96.
[16] K. Scrivener, Backscattered electron imaging of cementitious microstructures: understanding and quantification, Cement & Concrete Composites 26 (2004) 935–945.
[17] S. Speziale, H. Reichmann, F. Schilling, H. Wenk, P. Monteiro, Determination of the elastic constants of portlandite by Brillouin spectroscopy, Cement and Concrete Research 38 (10) (October 2008) 1148–1153.
[18] J. Chen, L. Sorelli, M. Vandamme, F.-J. Ulm, G. Chanvillard, A coupled nanoindentation/SEM-EDX study on low water/cement ratio portland cement paste: Evidence for C–S–H/CH nanocomposites, Journal American of Ceramic Society 93 (5) (2010) 1484–1493.
[19] M. Ashby, The deformation of plastically non-homogeneous materials, Philosophical Magazine 21 (170) (1970) 399–424.
[20] W. Nix, H. Gao, Indentation size effects in crystalline materials: a law for strain gradient plasticity, Journal of the Mechanics and Physics of Solids 46 (3) (1998) 411–425.
[21] Y. Huang, Z. Xue, H. Gao, W. Nix, Z. Xia, A study of microindentation hardness tests by mechanism-based strain gradient plasticity, Journal of Materials Research 15 (8) (2000) 1786–1796.
[22] J. Swadener, E. George, G. Pharr, The correlation of the indentation size effect measured with indenters of various shapes, Journal of the Mechanics and Physics of Solids 50 (2002) 681–694.
[23] N. Pugno, A general shape/size-effect law for nanoindentation, Acta Materialia 55 (2007) 1947–1953.
[24] J. Němeček, Creep effects in nanoindentation of hydrated phases of cement pastes, Materials Characterization 60 (9) (2009) 1028–1034.
[25] B. Budiansky, On the elastic moduli of some heterogeneous materials, Journal of the Mechanics and Physics of Solids 13 (1965) 223–227.
[26] R. Hill, A self-consistent mechanics of composite materials, Journal of the Mechanics and Physics of Solids 13 (1965) 213–222.
[27] P. Modal, S.P. Shah, L. Marks, A reliable technique to determine the local mechanical properties at the nanoscale for cementitious materials, Cement and Concrete Research 37 (2007) 1440–1444.
[28] P. Modal, S.P. Shah, L. Marks, Nano-scale characterization of cementitious materials, ACI Materials Journal 105 (2) (2008) 174–179.